Simultaneous Patterning of Two Different Types of Nanoparticles into Alternating Domains of a Striped Array of a Polymer Blend in a Single Spin-Casting Step

Saman Harirchian-Saei,[1] Michael C. P. Wang,[2] Byron D. Gates,[2] and Matthew G. Moffitt[*1]

Department of Chemistry, University of Victoria, P.O. Box 3065, Victoria, BC, V8W 3V6, Canada;[1] Department of Chemistry, Simon Fraser University, 8888 University Drive, Burnaby, BC, V5A 1S6 Canada.[2]

Abstract

A fast and convenient method is developed for simultaneously patterning inorganic nanoparticles with different optical, electronic or magnetic functionality to specific surface regions, by spin-casting onto microcontact printed substrates blend solutions in which the two nanoparticle types are functionalized with surface polymer brush layers of different surface energies. The process is based on phase separation of different nanoparticles based on their immiscible brush layers during spin-casting, with the underlying surface energy heterogeneity of the patterned substrate directing the different NP types to domains of different surface energies. Here, we specifically demonstrate the simultaneous localization of cadmium sulfide quantum dots (CdS QDs), addressed with a surface layer of polystyrene (PS), and silver nanoparticles (Ag NPs), addressed with a surface layer of poly(methyl methacrylate) (PMMA), onto the non-polar and polar surface domains, respectively, of hydrophilic glass patterned with hydrophobic octadecyltrichlorosilane (OTS) stripe arrays with micron-scale periodicities. In order to prevent gelation of solvent-swollen polymer-brush coated NPs during spin casting, which effects strong kinetic constraints on phase separation and localization, PS, PMMA or PS/PMMA homopolymer blends of sufficiently high M_w were added to the NP blends to increase the free volume between approaching NPs. The process parameters were fine-tuned to obtain control over defects in the obtained patterns .

Introduction

Organizing nanoparticles (NPs) into micro- and nanoscale structures on surfaces has various applications in medical diagnostics,[1,2] sensing,[3,4] nano- and optoelectronic devices,[5,6] light emitting diodes,[7] and photovoltaics.[8] A variety of techniques have been applied to this challenge including scanning probe-related patterning techniques,[8-14] the use of optical tweezers to position NPs on surfaces,[15,16] microcontact printing,[7,17-21] layer-by-layer assembly techniques[22,23] and various other lithographic approaches.[24-28]

The ability to fabricate patterned structures of multiple NP types with different functionalities (such as optical properties) opens up many new routes to design micro and nanodevices. Hua et.al. employed a layer-by-layer assembly approach combined with lithography to obtain a pattern of two types of NPs, where each one is directed to the desired location on the surface to form striped pattern of NPs;[29] although this technique results in high precision patterning, it is a labor-intensive multistep process. Jamshidi et.al. developed an elaborate technique termed "nano-pen" to pattern multiple NPs using optoelectronic tweezers to collect and immobilize them into patterned structures via electrokinetic forces.[30] Vossmeyer et.al. reported a selective deposition technique for patterning multiple NP types through selective deposition of each NP type onto chemically distinct interaction sites of a substrate, which was prepared by lithographic masking.[31] However, there is still the need for a fast, simple and efficient approach to patterning structurally- and compositionally-complex NP containing films.

Microcontact printing (μCP) is a convenient technique for patterning colloids, polymers and NPs.[32-36] Here, we develop a versatile technique based on μCP for simultaneous patterning of multiple NP types to discrete surface locations using a facile single-step spin-casting process. Our method is based on directed phase separation of polystyrene/poly(methyl methacrylate)

(PS/PMMA) blend films[37-49] via spin-casting onto pre-patterned octadecyltrichlorosilane (OTS) on glass, as developed previously in our group.[36] Also in that work, the methodology was extended to patterning of CdS quantum dots (QDs), by replacing PS homopolymer within the spin-cast solution with PS-coated CdS QDs (PS-CdS); the QDs possessed similar surface energy to the PS homopolymer and therefore localized selectively above the OTS lines. In this paper, this technology is further extended to include the simultaneous patterning of PS-CdS QDs--that should be directed to the lower-surface energy OTS lines of the substrate--and PMMA-coated Ag NPs (PMMA-Ag), which should be directed to the higher-surface energy regions between the OTS lines. Our main interest in polymer-supported patterns of Ag NPs and CdS QDs is to provide a suitable proof-of-concept system for simultaneous creation of patterns containing multiple NPs. However, this specific combination of NPs also exhibits interesting optical behaviour as a result of QD-surface plasmon interactions, which will be discussed in a forthcoming publication.

Experimental

Materials. Three different PS homopolymer samples with molecular weights (M_w) of 131,000 g/mol (previously synthesized in our group by anionic polymerization), 33,000 g/mol (Polymer Source Inc.) and 6000 g/mol (Polymer Source Inc.) were used for mixing with the NP blends; they are denoted in the text as PS 131k, 33k and 6k, respectively. PMMA homopolymer with M_w = 120,000 g/mol (denoted as PMMA 120k) was also used as received from Aldrich.

Synthesis of PS-Coated CdS Quantum Dots (PS-CdS). The polystyrene-coated CdS QDs (PS-CdS) used in this work is similar to that described in previous work from our group.[50-53] In summary, QDs were synthesized via templated growth of CdS in the cores of reverse micelles consisting of polystyrene-*block*-poly (acrylic acid) copolymer PS(226)-*b*-PAA(22),

where numbers in brackets indicate number-average degrees of polymerization for each block. The core of each PS-CdS contains a ~5 nm CdS nanoparticle (determined from UV-vis and using Henglein's empirical relationship),[54,55] with a poly(cadmium acrylate) (PACd) layer at the CdS surface, covalently-attached to a solubilized external PS brush layer.

Synthesis of PMMA-Coated Silver Nanoparticles (PMMA-Ag). For the synthesis of poly (methyl methacrylate)-coated silver nanoparticles (PMMA-Ag), poly (methyl methacrylate)-*block*-poly (acrylic acid) copolymer, PMMA(170)-*b*-PAA(28), where numbers in brackets indicate number-average degrees of polymerization for each block, was purchased from Polymer Source Inc. Silver acetate 99.99%, sodium borohydride ($NaBH_4$) and methanol (99.8+ %) were purchased from Aldrich. Reagent grade THF was purchased from Anachemia.In order to prepare PMMA-Ag, first a 2 wt % solution of PMMA(170)-*b*-PAA(28) was prepared in reagent grade THF and stirred for 3 h. In the meantime, a 0.25 M suspension of silver acetate in deionized (DI) water was prepared and a stoichiometric amount (measured as 1 Ag^+ to 1 acrylic acid repeat unit) was added quickly in a single shot from a volumetric pipette to the copolymer solution with constant and rapid stirring. The reason for adding silver acetate from a concentrated suspension was to keep the amount of water in the reaction solution at a minimum, in order to avoid precipitation of copolymer from the THF solution. The reaction solution immediately turned from clear and colourless to turbid bluish indicating the formation of micelles. After 1 h stirring, the reducing agent, which is 0.50 M aqueous solution of $NaBH_4$, was added to the solution in variable excess amounts relative to the molar amount of added silver acetate. Reduction of Ag^+ to Ag results in a color change of the solution to dark yellow. The solution was stirred overnight and then precipitated into cold methanol. The collected precipitate

was washed with methanol several times and dried overnight under vacuum. This procedure is illustrated by the schematic depiction in Figure 1.

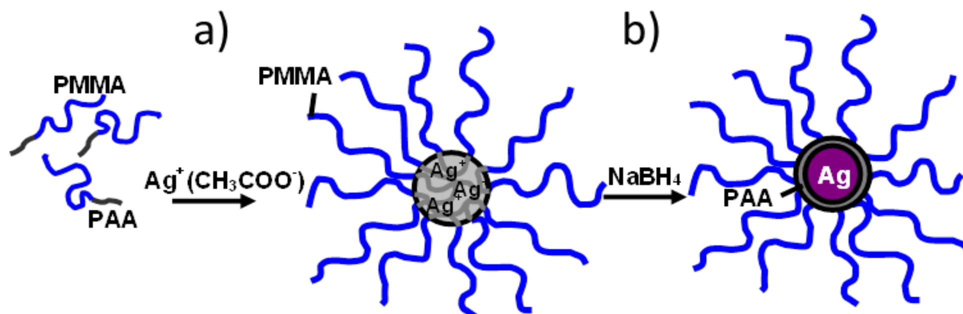

Figure 1. Synthesis of PMMA-Ag NPs: (a) micelle formation by the addition of silver acetate to the solution of PMMA-*b*-PAA in THF with soluble PMMA brush layer and insoluble Ag^{+}-containing PAA core; (b) Ag NP formation by reduction of Ag^{+} in the core to Ag^{0} using $NaBH_4$ as the reducing agent, forming the final PMMA-Ag nanoparticles.

Preparation of Polydimethylsiloxane (PDMS) Stamps for Microcontact Printing. Masters with microscale periodic stripe patterns were obtained using commercial compact discs (CDs). Top layers on a CD were removed revealing the underlying polycarbonate layer with the desired topographic features. The polycarbonate was used as the master, and a 10:1 (v/v) ratio of prepolymer to curing agent for polydimethylsiloxane (PDMS) (Dow Corning: Sylgard 184 DC-184 A and DC 184-B) were mixed and poured over the polycarbonate master. The PDMS was cured for 4 h at 80˚C. The topology of the resulting PDMS stamp consisted of periodic raised stripes corresponding to the troughs of the polycarbonate masters. The PDMS stamps were sonicated in a 1:2 (v:v) solution of ethanol/deionized water immediately prior to use.

Microcontact Printing of Glass Substrates with Octadecyltrichlorosilane (OTS). Glass cover slips (VWR scientific, 18 x 18 mm) were cleaned by sonication for 10 min in 95%

ethanol, followed by 10 min sonication in deionized water. To introduce a layer of hydroxyl groups on the glass surface, the coverslips were submerged in a piranha solution at 70 °C for 30 min. Piranha solution consists of a 3:1 (v/v) mixture of concentrated H_2SO_4 and 30% H_2O_2. (*Warning: piranha solution is a strong oxidizing agent, so extreme care is necessary when using it.*) Following piranha treatment, the coverslips were sonicated in DI water for 10 min and then rinsed with methanol, followed by two further repetitions of the sonication/rinsing process. The resulting hydrophilic glass substrates were dried with a UHP N_2(g) stream and used immediately for μCP. The ink for μCP was prepared by dissolving octadecytrichlorosilane (OTS, Aldrich) in anhydrous hexane (≥99%, Aldrich) under UHP N_2 (g) to obtain a 5 mM silane solution. For inking the PDMS stamp, an unpatterned smooth block of PDMS was used as an ink pad. One drop of the ink solution was spin-cast onto the pad at 3000 rpm for 30 s followed by 20 s drying under a stream of UHP N_2 (g). Then a PDMS stamp was brought into contact with the inked pad for 10 s. The inked PDMS stamp was then used to transfer the OTS molecules to the surface of a hydrophilic glass cover slip by a conformal contact for 30 s under a 200-g weight. The OTS-patterned glass substrates were used immediately for spin-casting the NP polymer blends.

Preparation of PS-CdS/PMMA-Ag Blend Solutions. Solutions of 0.5, 1.0, 2.0 and 4.0 wt % of PS-CdS and PMMA-Ag were prepared separately in spectro grade toluene (Aldrich) and stirred for 4 h then left overnight to equilibrate. The 30/70 and 50/50 (w/w) PS-CdS/ PMMA-Ag blend solutions were each prepared by gravimetrically mixing appropriate amounts of the two solutions (PS-CdS and PMMA-Ag) into a clean vial and actively stirring it for 4h. These solutions were left to equilibrate overnight.

As discussed in subsequent sections, in order to increase the characteristic length scale of the phase-separation in NPs blend films, homopolymers were added to the blends. Solutions of

0.5, 1.0 and 2.0 wt % PS-CdS, PMMA-Ag, PS, and PMMA were prepared separately in spectro grade toluene (Aldrich), stirred for 4 h, and left overnight to equilibrate. The 30/60/10 PS-CdS/PMMA-Ag/PMMA, 20/10/70 PS-CdS/PS/PMMA-Ag, 10/20/50/20 and 20/10/60/10 PS-CdS/PS/PMMA-Ag/PMMA blend solutions (all weight fractions) were each prepared by mixing the appropriate amounts of two solutions into a clean vial and stirring it for 4h then let it equilibrate overnight.

Preparation of Spin-Cast Films. One drop (~50 μL) of the blend solution was spin-cast onto a patterned or unpatterned glass coverslip for 30 or 60 s at either 3000, 6000 or 9000 rpm. The drop was applied after the substrate reached the desired spin speed. This droplet was deposited onto the centre of the spinning substrate using a microsyringe. Spin-cast films appeared uniformly transparent, and were dried overnight under vacuum prior to characterization, and subsequently stored in covered glass petri dishes kept in the dark.

For each composition and preparation condition, three separate samples of each film were prepared for a complete characterization to determine reproducibility of the process. Unpatterned glass substrates were cleaned prior to spin-casting by sonication in methanol, chloroform, toluene and acetone each for 10 min.

UV-Vis and FTIR Spectroscopy. UV-Vis measurements were performed on a CARY 5 UV-Vis-NIR spectrophotometer. Fourier transform infrared (FTIR) spectroscopy was performed on a Perkin Elmer Spectrum 1000 FTIR

X-Ray Diffraction (XRD). XRD measurements of Ag NPs was carried out using a Rigaku miniflex diffractometer operating with a Cr anode (Cr Kα1 λ=2.228970 Å) at 30 kV accelerating voltage and 15 mA electric current. The values for changes in 2θ were recorded

between 50° to 110° at a scan rate of 0.5°/min. Dry powders were ground and placed on a glass sample holder for these measurements.

Dynamic Light Scattering (DLS). DLS measurements were performed on a Brookhaven Instruments photon correlation spectrometer with a BI-200SM goniometer, a BI-9000AT digital autocorrelator, and a Melles Griot He-Ne Laser (632.8 nm) with a maximum power output of 75 mW. Samples for DLS measurements were prepared with extra care to avoid dust in the samples (dust scatter the light and result in imprecise measurement). 5 mg/mL stock solutions of PMMA-Ag were prepared in spectroscopic grade toluene and the solution was then equilibrated overnight. To remove dust, the solution was filtered after equilibration through two membrane filters with 0.45 μm nominal pore size connected in series. Subsequent dilution of the stock solution for DLS measurements was carried out by adding a known quantity of toluene filtered through two membrane filters with 0.45 μm nominal pore size connected in series.

DLS measurement of PMMA-Ag in toluene was conducted at a 90° scattering angle and at concentrations of 0.05 mg/mL. Three repeated measurements of the autocorrelation function were obtained and all DLS measurements were conducted at 23 °C.

Atomic Force Microscopy (AFM). AFM in contact mode was performed on a MFP-3D atomic force microscope from Asylum Research with non-conductive silicon nitride cantilevers from Veeco (model: NP-10). The cantilevers were 0.4 - 0.7 µm thick and their resonance frequency ranged from 12 to 75 kHz and with spring constants ranging from 0.06 to 0.58 N/m. For each sample, at least three images at different locations on the substrate were obtained to determine the regularity of the film structure. All images presented in this paper were scanned over a 10 µm x 10 µm area at a scan rate of 0.5 Hz and represent typical features observed for each film.

Transmission Electron Microscopy (TEM). TEM was carried out on a JEOL JEM-1400 electron microscope, operating at an electron accelerating voltage of 80 kV. Drop-cast samples were prepared by depositing a drop of 0.5 mg/mL PMMA-Ag solution in Toluene on a copper grid (300 mesh) coated with an amorphous carbon film; the grids were then dried at room temperature overnight before imaging. TEM images were collected at different magnifications and the particle size analysis was carried out on the samples at various regions of the TEM grid for a minimum of 90 particles.

Laser Scanning Confocal Fluorescence Microscopy (LSCFM). LSCFM measurements of patterned 1.0 wt % PS-CdS/PS/PMMA-Ag/PMMA 10/20/50/20 blend film were carried out on a Zeiss LSM 700 equipped with a diode laser. Films were excited at λ_{ex} = 480 nm, and emitted light above 520 nm was directed to the PMT detector by a variable dichroic filter. A Zeiss Plane-Aprochromat 63x oil-immersion objective lens (NA=1.3) was used for imaging. The pinhole diameter was set to 33 μm. To prepare samples for the LSCFM measurements, spin-cast blended films supported on a glass coverslip were taped to a glass microscope slide with the polymer film sandwiched between the slide and coverslip. Zeiss Immersionsoel 518 C oil was deposited between the objective lens and the coverslip in order to provide a constant-refractive index media between the objective lens and the glass coverslip.

Results and Discussion

Synthesis and Characterization of PMMA-*b*-PAAg Reverse Micelles. Poly(methyl methacrylate)-*block*-poly(silver acrylate) (PMMA-*b*-PAAg) micelle preparation is the first step in the synthesis of PMMA-Ag NPs, before the reduction of metal ions to form the encapsulated metal NP (Figure 1). The hydrodynamic radius (R_h) of the resulting micelles was measured in toluene by DLS; the average value between three runs resulted in R_h = 36 nm.

Synthesis and Characterization of PMMA-Ag Nanoparticles. The chemical reduction of silver-loaded reverse micelles to PMMA-stabilized Ag NPs results in the formation of NPs with size and properties that are dependent on the chemical conditions. An important factor that strongly affects the properties of the resultant NPs is the amount of reducing agent relative to the number of metal ions.[56] In this work, the reduction of Ag^+ to form NPs was performed using $NaBH_4$, which is a versatile reducing agent commonly used for Ag NP synthesis.[57,58] To ensure that $NaBH_4$ does not affect the polymeric stabilizer surrounding the NPs, FTIR spectra were collected for the PMMA-*b*-PAAg micelle sample before adding the reducing agent, as well as for PMMA-Ag after reduction using a 10x molar excess of reducing agent (i.e. 10 $NaBH_4$:1 Ag^+). Identical carbonyl stretching absorption peaks were observed for both spectra, indicating the polymer interacting with the surfaces of the NPs is largely unaffected during the reduction reaction.

To investigate the influence of the amount of the reducing agent on the properties of the synthesized NPs, three different samples were prepared each with a different amount of $NaBH_4$. PMMA-Ag prepared with 5x, 8x and 10x excess of the reducing agent relative to the molar amount of Ag^+ were prepared for this study. These samples are designated PMMA-Ag1,

PMMA-Ag2, PMMA-Ag3, respectively. A detailed characterization of all three samples is presented here.

The crystal structure of the Ag cores for PMMA-Ag1, PMMA-Ag2, and PMMA-Ag3 were characterized using XRD (Figure 2). For all three samples, the observed peaks match a crystal structure of *silver-3c syn* (pink traces shown on the XRD patterns).[59,60] This structure has been reported as a common structure for stable Ag NPs and is a face centre cubic structure with diffraction peaks at 2θ = 58°, 68° and 105° corresponding to the (111), (200), and (220) planes.[59,60] The XRD patterns also show additional peaks at 2θ = 65° and 83° which may be attributed to silver oxides or other impurities.[61] These two impurity peaks appeared much weaker for the PMMA-Ag3 sample, prepared using the largest relative amount of reducing agent.

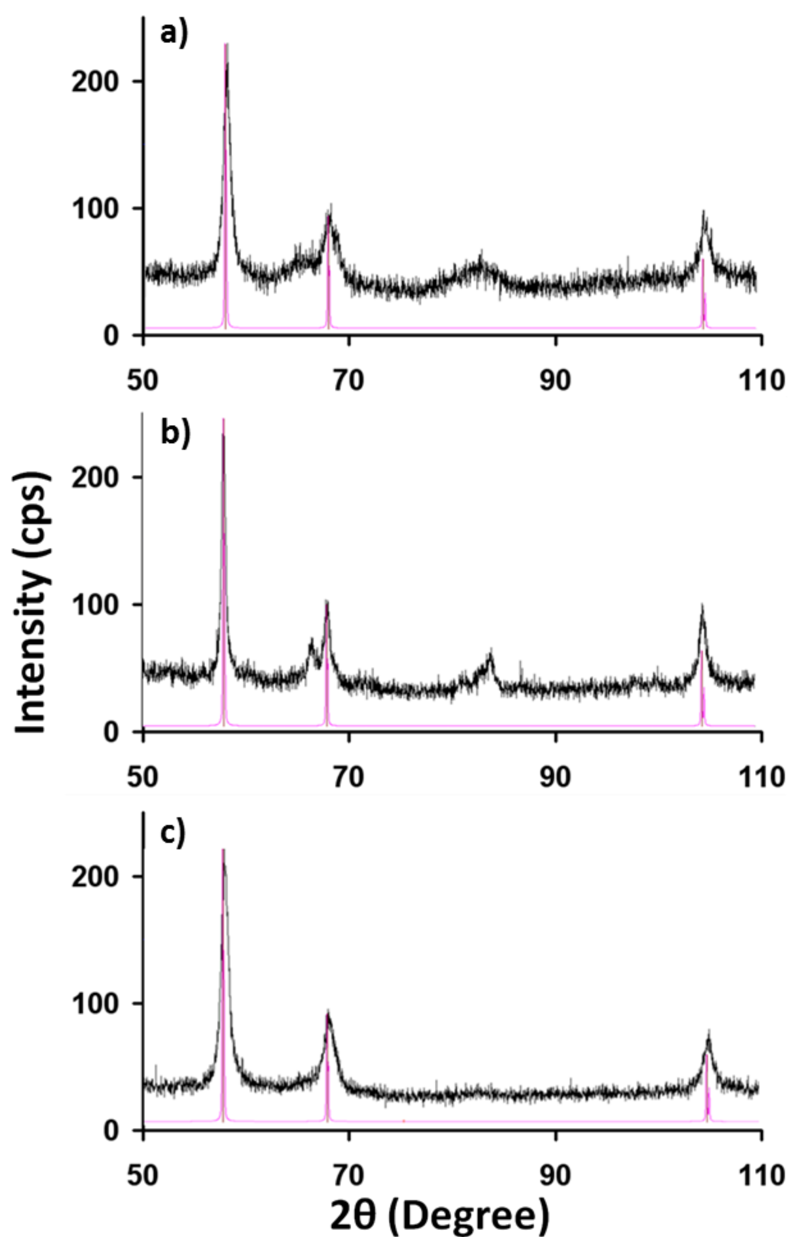

Figure 2. XRD diffraction patterns of (a) PMMA-Ag1, (b) PMMA-Ag2, and (c) PMMA-Ag3. Pink traces illustrate the anticipated crystalline pattern of the *silver 3c-syn* structure showing peaks at $2\theta = 58°$, 68° and 105° corresponding to the (111), (200), and (220) planes.

Hydrodynamic radii (R_h) of PMMA-Ag1, PMMA-Ag2, and PMMA-Ag3 were determined by DLS measurements. The average R_h values, calculated from three repeat DLS measurements for each sample, were: R_h = 41.7, 60.6 and 35.4 nm for the samples prepared

using a 5, 8, and 10x excess of the reducing agent, respectively. The shape and size distributions of the NPs were also assessed by TEM imaging along with a statistical analysis of these TEM images. Representative images of features observed for each of the three samples is provided in Figures 3a, c, and e.

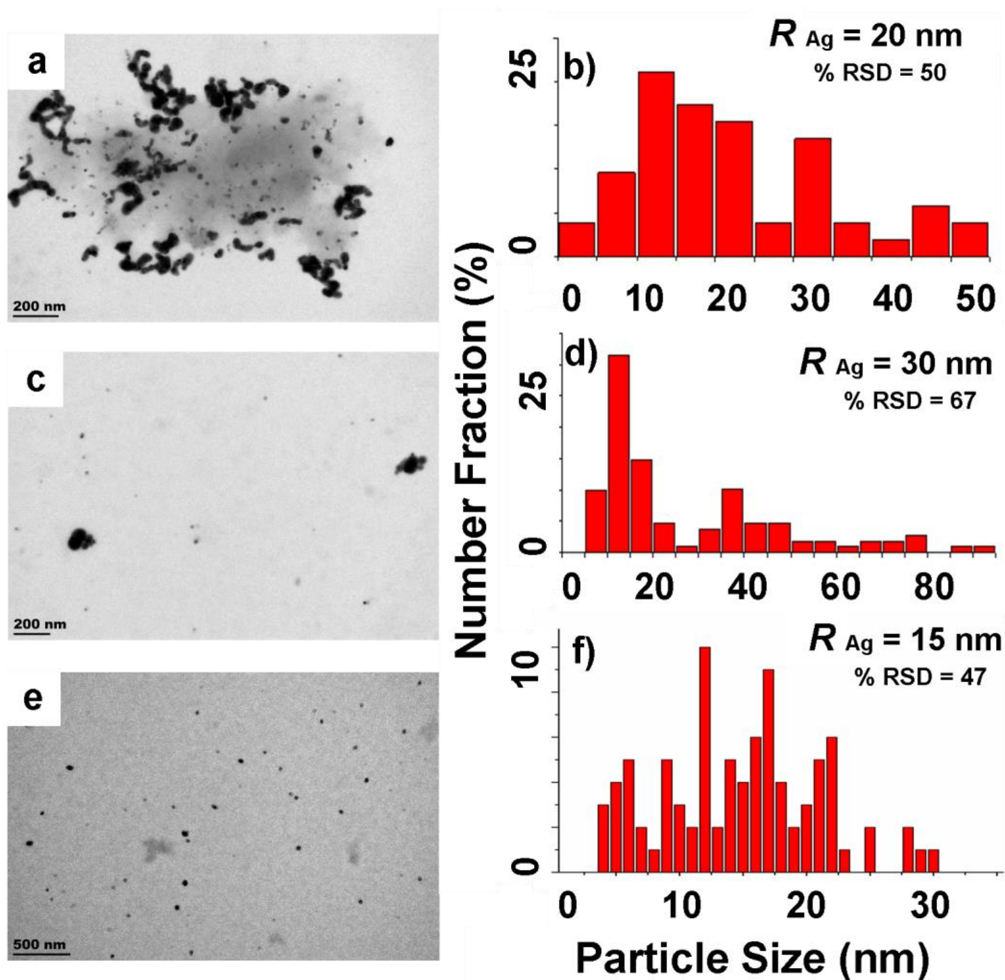

Figure 3. Representative TEM images (a, c, e) and the size distributions (b, d, f) of (a, b) PMMA-Ag1, (c, d) PMMA-Ag2 and (e, f) PMMA-Ag3. Average size of the NPs (radius, R_{Ag}) and percent relative standard deviation, % RSD, are both indicated on each histogram.

All TEM images show a distribution in the size of the Ag NPs. Statistical particle size measurement results in different distributions for each quantity of reducing agent used in

preparing the Ag NP cores (Figures 3b, d, and f). Average sizes of PMMA-Ag1, PMMA-Ag2, and PMMA-Ag3 NPs are R_{Ag} = 20, 30, and 15 nm, respectively. Comparing the widths of each distribution, the % RSD is the highest for the PMMA-Ag2 sample and the lowest for the PMMA-Ag3 sample.

DLS and TEM results both demonstrate that increasing the amount of reducing agent is causing first an increase and then a decrease in the size of NPs. This size analysis also indicates that the lowest polydispersity of NPs is obtained for the sample prepared using the largest amount of reducing agent (PMMA-Ag3). Another difference between the three PMMA-Ag NPs is their core morphologies. Nanoparticles prepared within block copolymer micelles use a smaller amount of reducing agent typically results in NPs with exclusively a "cherry-like" (one NP per micelle) morphology (Figure 4a). In contrast, ~8% of the cores prepared by the reduction reaction with the highest amount of reducing agent (10x excess) forms a "raspberry-like" morphology with many small NPs per micelle (Figure 4b). This difference can be understood based on the rates of nucleation for each sample. The PMMA-Ag3 sample would have the highest rate of nucleation corresponding to the highest amount of reducing agent, which can produce multiple nucleation sites per core.[56]

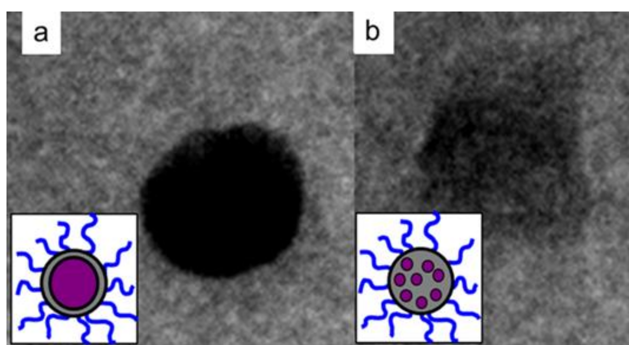

Figure 4. Demonstration of both (a) "cherry-like" and (b) "raspberry-like" NPs morphologies observed by TEM analysis of the PMMA-Ag3 samples. Inset schematics (edge lengths = 20 nm) demonstrate the difference between these two morphologies.

Extinction spectra for the three different PMMA-Ag NP samples reveal the shape and position of their surface plasmon (SP) bands (Figure 5). For the NPs prepared with the least amount of reducing agent (PMMA-Ag1), a broad SP band is observed at 407 nm. Increasing the amount of reducing agent to 8x (PMMA-Ag2) sharpens and shifts the peak to 417 nm. The sharpest SP peak (positioned at 419 nm) was observed for the sample prepared using 10x excess $NaBH_4$ (PMMA-Ag3). In all spectra, we also observed a shoulder at ~350 nm that became weaker with increasing amounts of reducing agent. This SP shoulder may be attributed to a broad Ag NP size distribution, which becomes narrower as the amount of added reducing agent increases, as shown in Figure 3.

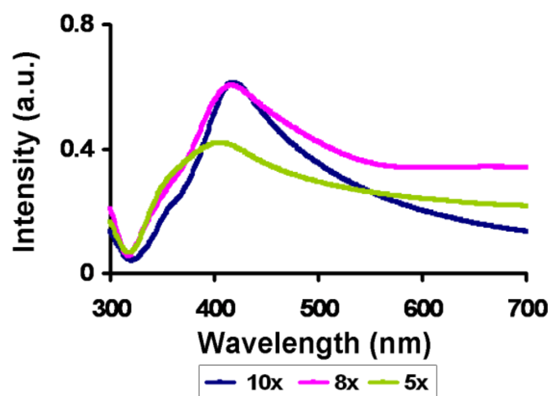

Figure 5. Extinction spectra of PMMA-Ag NPs (dispersed in toluene). The three samples were prepared using 5x (PMMA-Ag1), 8x (PMMA-Ag2), and 10x (PMMA-Ag3) excess $NaBH_4$.

Considering the various figures of merit for the PMMA-Ag samples described above, including crystalline purity, sharpness of the SP peak, and size and polydispersity of the particles, we used the samples prepared with 10x excess reducing agent (PMMA-Ag3) for the patterning experiments described in the remainder of this work. In summary, PMMA-Ag3 consists of Ag nanoparticles with mean radius of ~15 nm, a collapsed PAA layer on the surfaces of the Ag NPs, and a solvent-swollen covalently-attached PMMA corona (Figure 1). The hydrodynamic radius (R_h) of the particles in toluene is ~36 nm (suggesting a ~20 nm-thick

polymer layer surrounding each nanoparticle in solution) consisting of on average ~45 copolymer chains (from SLS).

Spin-Cast Films of PS-CdS/PMMA-Ag Blends on Unpatterned Glass Substrates. An essential requirement for patterning the desired polymer blend components onto a patterned substrate is that the length scale of phase separation in the spin-cast films is commensurate with the length scale of the underlying patterned features. Therefore, to first determine their characteristic length scales of phase separation, we investigated the morphologies of PS-CdS/PMMA-Ag blends spin-cast onto bare glass surfaces. These films were prepared via spin-casting blend solutions with a total polymer concentration c_p = 4.0 wt %, and either 30/70 or 50/50 (w/w) PS-CdS/PMMA-Ag in toluene. These solutions were cast onto unpatterned clean glass surfaces at spin speeds of either 3000, 6000 or 9000 rpm. Interestingly, and in contrast to spin-cast PS/PMMA homopolymer blends described in our previous work[36,62] and elsewhere,[38,40,45] AFM images of the PS-CdS and PMMA-Ag blend films (Figure 6) reveal relatively featureless topologies without developed PS/PMMA domain structures for all spin speeds and for both compositions. The rare surface features that are observed in these images are probably dust or other impurities. The absence of microscale domain features on the surfaces of the blend films should not be a result of insufficient interfacial tension between blend components. The PS/PMMA and PS-CdS/PMMA-Ag pairs should have very similar interaction energies and the PS/PMMA blends have been shown to exhibit well developed phase structure under identical spin-casting conditions. Rather, as discussed below, we attribute this absence of phase-separation in the NP blends to the difference in structure between homopolymers and polymer-coated NPs. This absence of phase-separated structure on the micron-scale in the spin-

cast PS-CdS/PMMA-Ag blends precludes their patterning on microcontact printed surfaces and, therefore, must now be addressed.

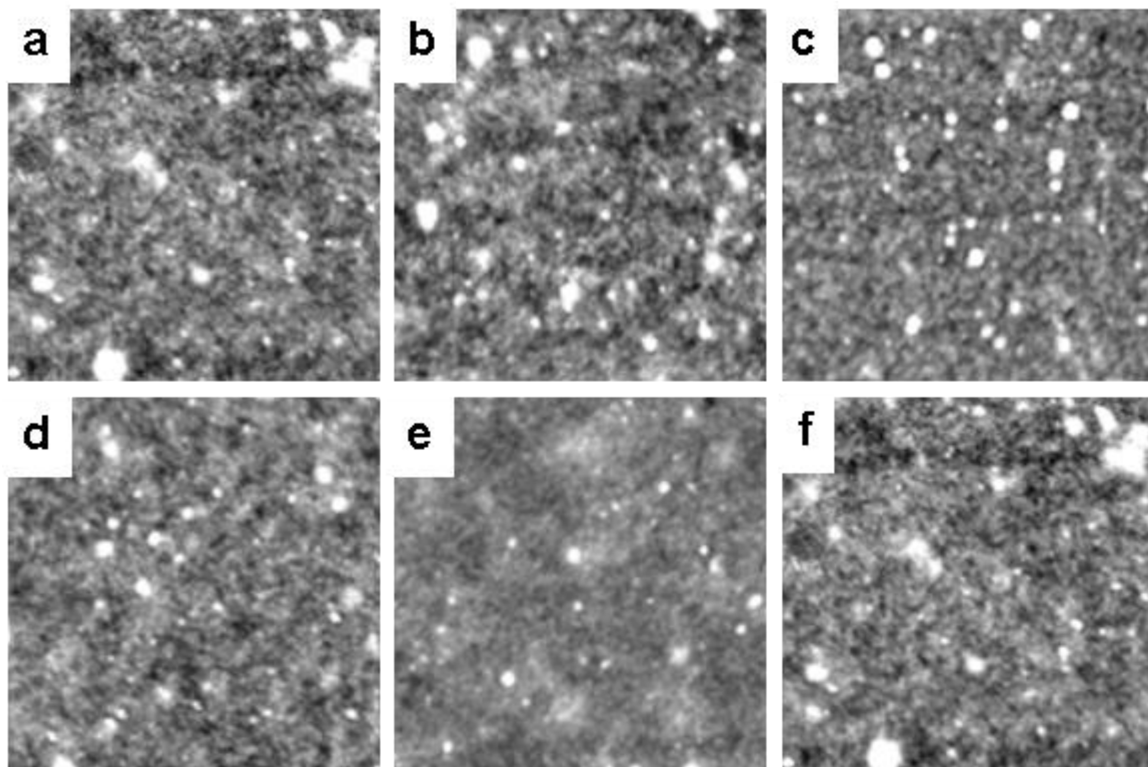

Figure 6. 10 x 10 μm AFM images of 4.0 wt % 30/70 (a-c) and 50/50 (d-f) PS-CdS/PMMA-Ag samples spin-cast at (a, d) 3000, (b, e) 6000 and (c, f) 9000 rpm onto unpatterned glass slides.

To understand the absence of phase-separated structure in these blends, we consider what happens within the spin-cast solutions as the solvent evaporates. Both PS-CdS and PMMA-Ag NPs can be described as spherical polymer brushes. The PS or PMMA chains are attached at one end to relatively small and compact NP cores, resulting in a large, expanded, and highly solvent-swollen coronae. The interactions between spherical polymer brushes, in the form of reverse block copolymer micelles in organic solvents, have been described in detail by Gast and coworkers.[63-65] At micelle volume fractions above the critical overlap concentration, the steric repulsion between overlapping coronal chains of approaching micelles effects repulsive "soft-

sphere" intermicellar interactions, leading to micelle ordering into a body-centered cubic (BCC) lattice. Such ordering has been found to effect gel formation with a dramatic increase in viscosity and extremely limited particle mobility. We believe similar gelation of PS-CdS/PMMA-Ag NPs as the solvent evaporates during spin-casting leads to their highly restricted mobility, providing a strong kinetic constraint on domain formation and growth despite the thermodynamic driving force for PS-CdS and PMMA-Ag NPs to phase separate. In other words, once the PS-CdS and PMMA-Ag NPs are "frozen" into a gel, they have very limited translational mobility and cannot, therefore, segregate into microscale phase domains before the solvent is completely depleted and the polymer blend becomes vitrified. A schematic of gelation of toluene-swollen PS-CdS and PMMA-Ag NPs into a BCC array at a point in the spin-casting process when the extent of toluene evaporation is sufficient for neighboring brushes to overlap but insufficient to trigger phase separation, is represented in Figure 7a; here, the PS- and PMMA-coated particles are shown to be statistically mixed within the gel due to their common solvation by toluene. Subsequent to the time represented in Figure 7a, continued removal of toluene will make phase separation between PS-CdS and PMMA-Ag thermodynamically favourable, although the slow dynamics of the gel state will severely limit the length scale over which phase domains can develop.

Spin-Cast Films of PS-CdS/PMMA-Ag Blends with Added Homopolymer on Unpatterned and Patterned Glass Substrates. In order to prevent gelation of the PS-CdS and PMMA-Ag NPs, we decided to add PS, PMMA, or a mixture of PS/PMMA homopolymers to the blend solutions prior to spin-casting. The idea is to increase the free volume between NPs and to prevent the overlap of approaching NP brushes and the resulting soft-sphere ordering during solvent evaporation by adding homopolymer to the spaces in between the brushes. To

investigate the effect of added homopolymer on the phase-separation, we first added PS homopolymer with three different M_w values of 6k, 33k and 131k g.mol^{-1}, each at 10 wt % relative to the total polymer composition, while maintaining a PS (PS + PS-CdS)/PMMA (PMMA-Ag) ratio of 30/70 (w/w). The three resulting blends are described as PS (6k, 33k, or 131k)/PS-CdS/PMMA-Ag 10/20/70 (w/w/w). All blends were spin-cast at a polymer concentration of c_p = 1.0 wt %. Since Figure 6 shows PS-CdS/PMMA-Ag blends spin-cast at 4.0 wt %, we also carried out the control experiment at c_p = 1.0 wt % for the blend without added PS; similar to the 4.0 wt % case, no discernible phase separation on the micron-scale was observed by AFM analysis in these control c_p = 1.0 wt % blends.

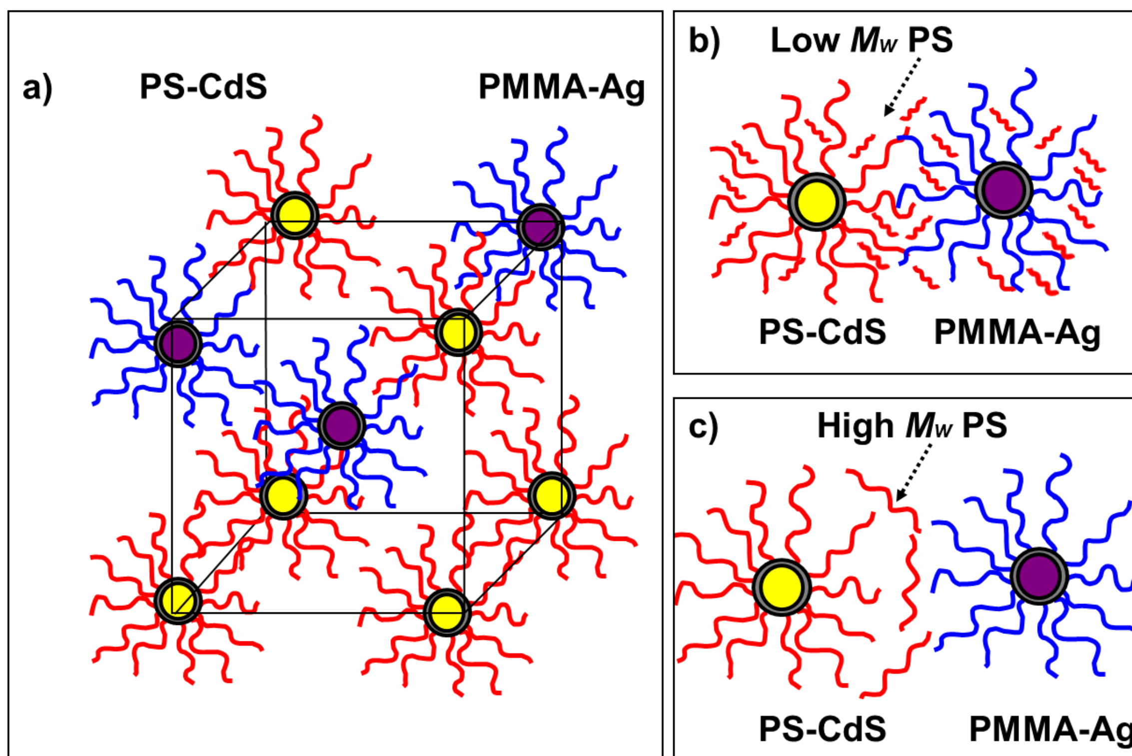

Figure 7. Schematic describing (a) NP blend ordering and gelation above a critical overlap concentration, (b) addition of low-M_w PS to the NP blend forming a "wet-brush" blend, and (c) addition of high-M_w PS to the NPs blend forming a "dry-brush" blend. As discussed in the text, the (c) case is more effective at preventing gelation and promoting phase separation, since it leads to increased free volume and greater separation between approaching spherical brushes.

In contrast to Figure 6, AFM of various blends on clean glass (Figure 8, a to c) show that the addition of PS homopolymer increases the extent of phase-separation and that the size of the resulting phase domains increases as the M_w of the added homopolymer increases. Specifically, very fine but difficult to measure domains were observed in the PS(6k) blend, whereas the measured average domain sizes increased to 0.2 ± 0.1 μm and then to 0.4 ± 0.1 μm in the PS(33k) and PS(131k) blends, respectively. The observed trends suggest that higher M_w homopolymer increase the particle mobility (by impeding gelation) to a greater extent than lower M_w homopolymer. This trend is explained by the relative tendency of different sized homopolymers to intercolate into the solvent-swollen brushes of the NPs. It is found that when the homopolymer is on the same order or greater than the size of the brush chains, there is an entropic tendency for the chains to be excluded from the brush and occupy the interparticle spaces; this is referred to as the "dry brush" case.[66-68] Conversely, when the M_w of added homopolymer is smaller than that of the similar polymer brush, the homopolymer gets included in the brush; this is referred to as the "wet brush" case. In our system, the NP mobility should be increased to a greater extent when most of the homopolymer is localized between the NPs ("dry brush" case) rather than within the brushes ("wet brush" case), since the former case has a more direct and clear influence on increasing the separation between NPs, thus preventing interparticle overlap and ordering. This explains the relative increase in the characteristic length scale of phase separation, d, as a function of increasing PS M_w added to the blends (Figure 8, a-c). Schematics describing the effects of adding low and high M_w homopolymer to the NP blends are illustrated in Figure 7, b and c, respectively.

Figure 8, d-f illustrates the corresponding film morphologies of PS-CdS/PS/PMMA-Ag on OTS-patterned surfaces. The inset to Figure 8d shows an AFM image of the substrate of OTS

lines on glass used for spin-casting in Figure 8, d-f, with pattern dimensions as described in ref. 36: $\lambda = 1.4 \pm 0.1$ µm, $w_s = 0.4 \pm 0.1$ µm and $w_l = 1.0 \pm 0.1$ µm. For added 6k and 33k PS (Figure 8, d and e), the polymer surface topology did not reveal the underlying surface pattern, because the characteristic length scale of phase separation, d, is still not large enough relative to the underlying pattern features. However, for the blend with added 131k PS, which has the largest d in this series, patterned lines were observed in the form of depressions above the underlying OTS stripes (Figure 8f). This result suggests a dewetting of the spin-cast blends from these stripes. The volume fraction of the PS/PS-CdS phase, however, does not match the observed surface stripes, meaning that phase separation and NP localization is not complete and that both PS and PMMA components are present in the regions in between the OTS lines.

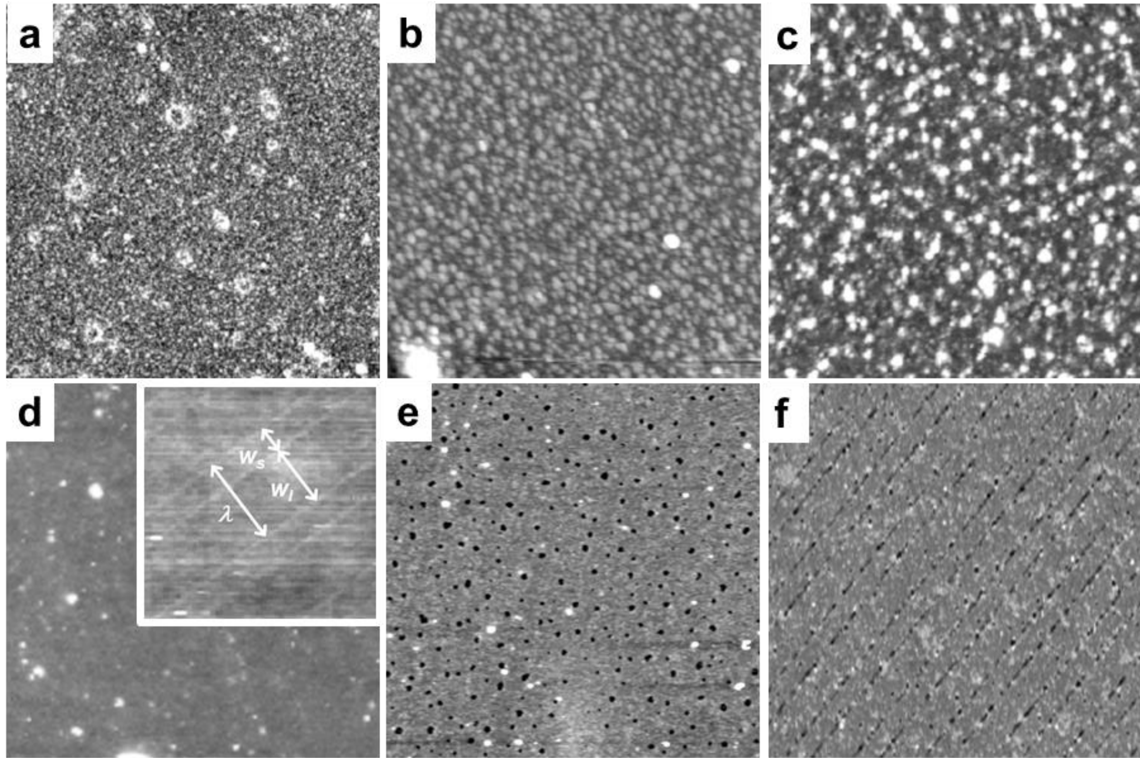

Figure 8. 10 x 10 μm AFM images of 1.0 wt % 20/10/70 (w/w/w) PS-CdS/PS/PMMA-Ag films prepared using (a, d) 6 k, (b, e) 33 k and (c, f) 131 k PS homopolymer. Films spin-cast at 6000 rpm from toluene on unpatterned (a-c) and OTS-patterned substrates (d-f). The inset to (d) shows an AFM image of the substrate of OTS lines on glass used for spin-casting in (d)-(f), with pattern dimensions as described in ref. 36: $\lambda = 1.4 \pm 0.1$ μm, $w_s = 0.4 \pm 0.1$ μm and $w_l = 1.0 \pm 0.1$ μm.

The effect of added homopolymer is also demonstrate for NP blends with added 10 wt % PMMA with M_w = 120k homopolymer. Films were prepared using 1.0 wt % 30/60/10 (w/w/w) PS-CdS/PMMA-Ag/PMMA on unpatterned and OTS-patterned substrates (Figure 9, a and b). Similar to the case of adding high-M_w PS, d has increased relative to the pure PS-CdS/PMMA-Ag blends ($d = 0.4 \pm 0.1$ μm) and the pattern lines were also observed in the blend film when spin-cast onto the patterned substrate. The similar results observed for high-M_w PS and high-M_w PMMA suggest that the specific chemical nature of the added homopolymer is relatively unimportant in this strategy since both PS and PMMA homopolymers are soluble in toluene

during the spin-casting process and, therefore, equally capable of increasing the separation between the approaching spherical brushes.

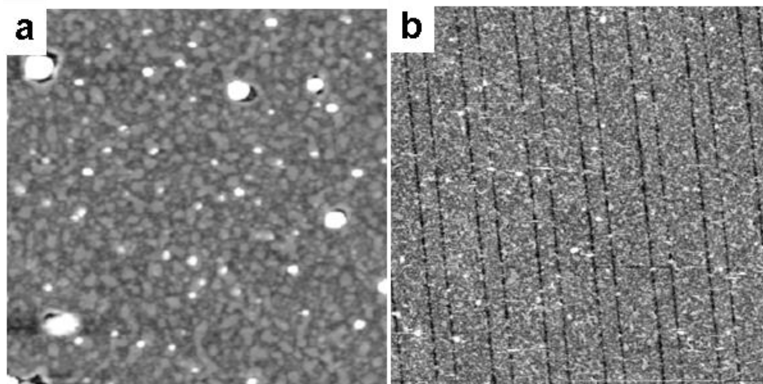

Figure 9. 10 x 10 μm AFM images of c_p = 1.0 wt % 30/60/10 (w/w/w) PS-CdS /PMMA-Ag/PMMA films prepared using 120 k PMMA. Films spin-cast at 6000 rpm from toluene onto (a) unpatterned and (b) OTS-patterned substrates.

As described in our previous work,[36] the characteristic length scale of phase separation, *d*, can be adjusted by fine-tuning the polymer concentration c_p of the blend and the spinning speed at which the films are prepared. Therefore, we studied the morphology of the blend films with added 10% of either 133k PS or 120k PMMA on OTS-patterned substrates for solution concentrations of 0.5, 1.0 or 2.0 wt % and spin speeds of 3000, 6000 or 9000 rpm. For all of these cases, either the polymer surface topology did not reveal the underlying surface pattern, or "dewetted" morphologies with incomplete phase separation, similar to those shown in Figures 8f and 9b were obtained. This indicated that the blend composition had to be further modified in order to obtain the desired localization of different types of NPs within distinct features in the achieved pattern. Our next step was, therefore, to add *both* 10% of high-M_w PS homopolymer *and* 10% of high-M_w PMMA homopolymer to further increase the free volume and facilitate phase separation (maintaining a total PS/PMMA ratio of 30/70). AFM images of spin-cast films of the resulting blend 20/10/60/10 (w/w/w/w) PS-CdS/PS/PMMA-Ag/PMMA on OTS-patterned

substrates are shown in Figure 10 for total polymer concentrations of c_p = 0.5, 1.0 and 2.0 wt % and spin speeds of 3000, 6000 and 9000 rpm.

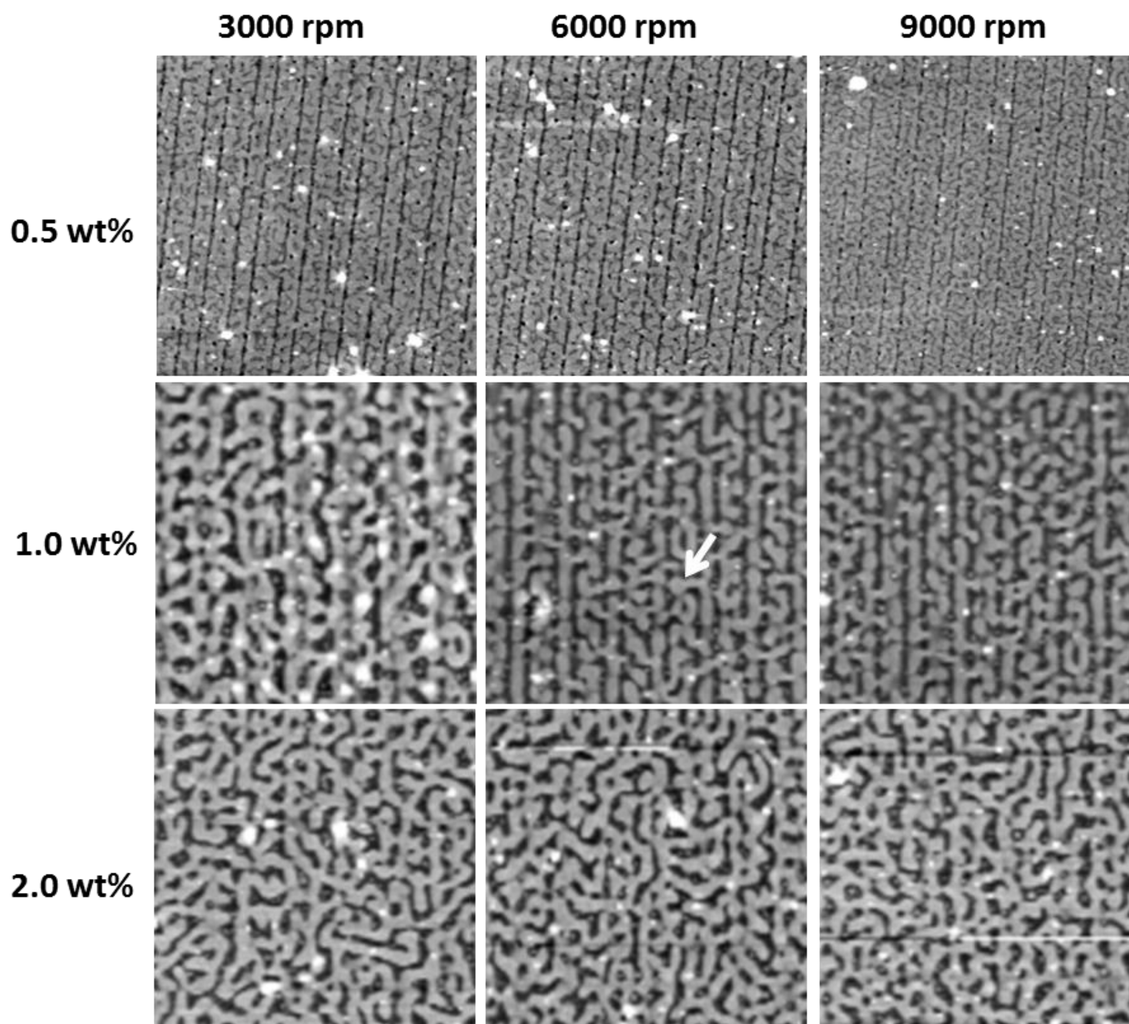

Figure 10. 10 x 10 μm AFM images of c_p = 0.5, 1.0 and 2.0 wt % 20/10/60/10 PS-CdS/PS/PMMA-Ag/PMMA (w/w/w/w) films spin-cast at 3000, 6000 and 9000 rpm from toluene onto OTS patterned substrates. An example of bridging between the raised domains is indicated with an arrow on the AFM image for 6000 rpm and 1.0 wt %.

The addition of both types of homopolymers at once results in phase-separated NP domains that are considerably larger than in previous cases (Figure 10). Average measured *d* for

c_p = 0.5, 1.0 and 2.0 wt % blend films spin-cast at 6000 rpm are 0.2 ± 0.1, 0.5 ± 0.1, and 0.7 ± 0.1 µm, respectively. For c_p = 0.5 wt %, small phase domains of both PS and PMMA are observed in the regions in between the OTS lines for samples prepared at all three spin speeds. For c_p = 1.0 wt % raised PMMA domains are elongated in a direction parallel to the pattern and connected by some bridges (as the one highlighted with a red dashed box) that span the OTS lines of the underlying substrate. For c_p = 2.0 wt %, domain shapes are mostly irregular with little elongation corresponding to the direction of the pattern. The best pattern replication in this series is obtained for the c_p = 1.0 wt % blend cast at higher spin speeds (6000 and 9000 rpm). However, even for these cases, the raised domains are not discrete and they are connected through bridges.

Finally, we improved the pattern replication and NP localization within the spin-cast blends even further by increasing the amount of both PS and PMMA homopolymers from 10 to 20 wt %. For the blend of 10/20/50/20 PS-CdS/PS/PMMA-Ag/PMMA (w/w/w/w), pattern replication was obtained for both c_p = 0.5 and 1.0 wt % blends. Low magnification AFM images (50 x 50 µm, shown in Figure 11) demonstrate the long-range patterning of these blends. The improvement is more obvious for the 1.0 wt % case (Figure 11b), which shows the least number of bridging defects in the patterned domains. We note that high (light) and low (dark) regions in the observed topological AFM images should correspond to phase-separated PMMA and PS domains, respectively. It is well established that when PS/PMMA blends are spin-cast from toluene, the PS domains will be more highly solvent-swollen and, therefore, collapse to a lower height upon final removal of solvent. The resulting areas of high and low regions in Figure 11b also appear to correspond to the 30/70 ratio of the respective components in the blend. Since CdS QDs and Ag NPs will be localized in the PS and PMMA domains, respectively, due to their

distinct surface coatings, the AFM image is Figure 11b suggests a successful simultaneous patterning of CdS QDs and Ag NPs into discrete domains of a striped array covering a large area and accomplished in a single, fast spin-casting step.

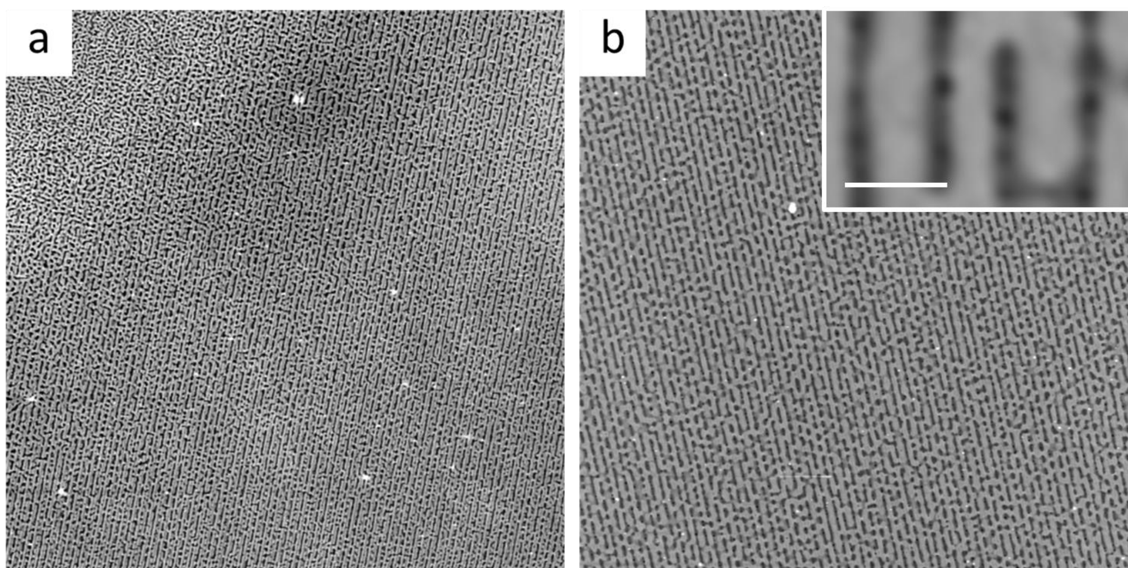

Figure 11. 50 x 50 µm AFM images of (a) c_p = 0.5 and (b) c_p = 1 wt % of 10/20/50/20 PS-CdS/PS/PMMA-Ag/PMMA (w/w/w/w) films spin-cast at 6000 rpm from toluene on OTS patterned substrates. The inset in (b) shows a detail of the same film at high magnification, which the scale bar = 1 µm

To confirm the identity of the domains and the proposed localization of QDs and NPs, LSCFM imaging was performed to probe the localized photoluminescence of the QDs from the regions to where they are directed during the spin-casting process. The excitation and emission filters for LSCFM were selected according to the photoluminescent properties of the constituent PS-CdS QDs. A representative LSCFM image of the same film shown in Figure 11b (see Figure 12b) clearly shows localized CdS emission in the expected OTS regions of the striped array. The periodicity of bright and dark stripes are similar to that of the underlying OTS pattern (Figure 8d, inset): λ = 1.4 ± 0.1 µm, w_s = 0.4 ± 0.1 µm and w_l = 1.0 ± 0.1 µm; comparison of the spacing

between the bright photoluminescent lines in the LSCFM image and in the underlying OTS pattern suggests the registration of CdS-containing PS domains to the OTS lines. These data are, therefore, consistent with the lateral distribution of photoluminescent CdS QDs and non-photoluminescent Ag NPs depicted in Figure 12a.

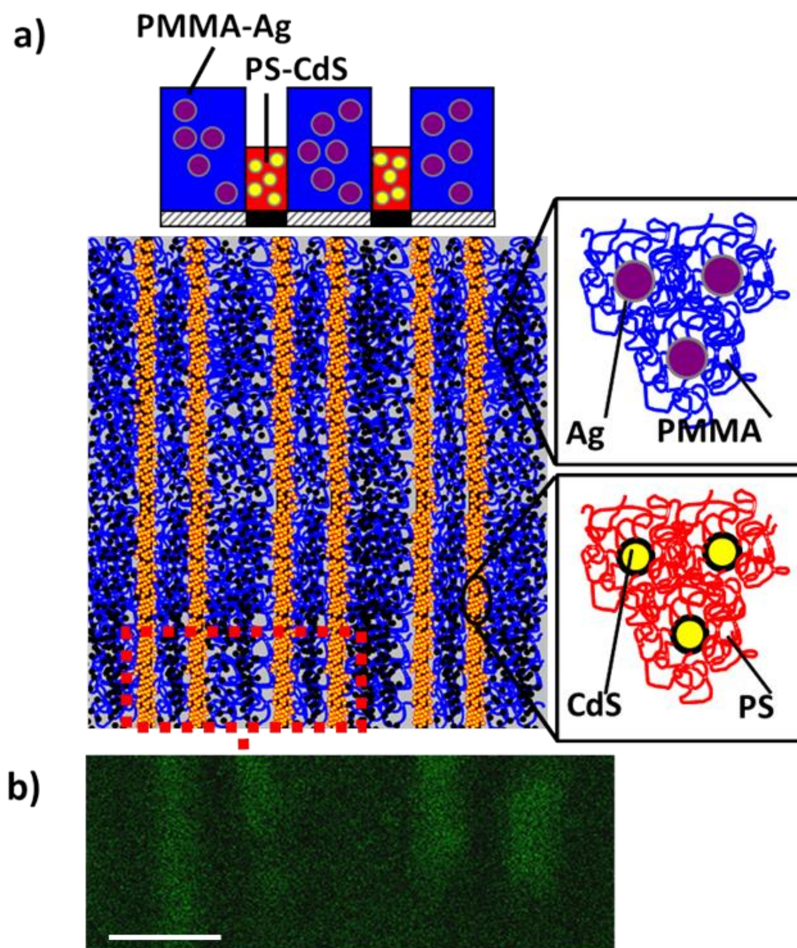

Figure 12. (a) Selective localization of PS-CdS and PMMA-Ag within the low- and high-energy regions of the OTS-patterned substrate. (b) LSCFM image of the c_p = 1.0 wt % 10/20/50/20 PS-CdS/PS/PMMA-Ag/PMMA (w/w/w/w) blend spin-cast at 6000 rpm from toluene onto OTS patterned substrates. Scale bar is 1 μm.

Conclusions

In this work, we developed a fast, single-step methodology to simultaneously pattern two types of inorganic NPs (e.g., CdS QDs and Ag NPs) by spin-casting onto chemically-patterned substrates, which were prepared by microcontact printing OTS onto hydrophilic glass. This process is based on surface energy heterogeneity of the patterned substrate that directs the specific NP types according to the surface energies of their respective polymer brush layers. One challenge addressed in this work was the gelation of solvent-swollen polymer-brush coated NPs during spin-casting and solvent evaporation, which introduced a strong kinetic constraint on the phase separation and subsequent localization of different NP types. This constraint was successfully lifted by adding PS, PMMA or PS/PMMA homopolymers of sufficiently high M_w to the NPs blends to increase the separation between approaching spherical brushes, preventing gelation and thus allowing phase separation and nanoparticle localization to occur. Pattern replication was then fine-tuned by changing variables, such as solution concentration and spinning speed, to obtain distinct nanoparticle-containing domains that were addressed to specific regions of underlying OTS-patterned substrate. We believe that this methodology is general and flexible, and can be applied to patterning different types of NPs into a wide variety of device-oriented polymer/nanoparticle hierarchical structures.

Acknowledgement

The authors gratefully acknowledge the Natural Science and Engineering Research Council (NSERC), the Canada Research Chairs Program, the Canadian Foundation for Innovation (CFI), and the British Columbia Knowledge Development Fund (BCKDF) for their generous support of the research. This work also made use of 4D LABS shared facilities

supported by CFI, BCKDF, Western Economic Diversification Canada, and Simon Fraser University.

Supporting Information

Sample AFM images with vertical scale bars from each figure; vertical scale bars for all AFM images within a figure are identical, with the exception of the inset to Figure 8d.

References

(1) Brown, P. O.; Botstein, D. *Nat. Genet.* **1999**, *21*, 33.

(2) Schena, M.; Shalon, D.; Davis, R. W.; Brown, P. O. *Science* **1995**, *270*, 467.

(3) Anker, J. N.; Hall, W. P.; Lyandres, O.; Shah, N. C.; Zhao, J.; Van Duyne, R. P. *Nat. Mater.* **2008**, *7*, 442.

(4) Hoa, X. D.; Martin, M.; Jimenez, A.; Beauvais, J.; Charette, P.; Kirk, A.; Tabrizian, M. *Biosens. Bioelectron.* **2008**, *24*, 970.

(5) Huang, M. H.; Mao, S.; Feick, H.; Yan, H. Q.; Wu, Y. Y.; Kind, H.; Weber, E.; Russo, R.; Yang, P. D. *Science* **2001**, *292*, 1897.

(6) Javey, A.; Guo, J.; Wang, Q.; Lundstrom, M.; Dai, H. J. *Nature* **2003**, *424*, 654.

(7) Rizzo, A.; Mazzeo, M.; Palumbo, M.; Lerario, G.; D'Amone, S.; Cingolani, R.; Gigli, G. *Adv. Mater.* **2008**, *20*, 1886.

(8) Wouters, D.; Schubert, U. S. *Angew. Chem. Int. Edit.* **2004**, *43*, 2480.

(9) Piner, R. D.; Zhu, J.; Xu, F.; Hong, S. H.; Mirkin, C. A. *Science* **1999**, *283*, 661.

(10) Ginger, D. S.; Zhang, H.; Mirkin, C. A. *Angew. Chem. Int. Edit.* **2004**, *43*, 30.

(11) Salaita, K.; Wang, Y. H.; Mirkin, C. A. *Nat. Nanotechnol.* **2007**, *2*, 145.

(12) Li, B.; Goh, C. F.; Zhou, X. Z.; Lu, G.; Tantang, H.; Chen, Y. H.; Xue, C.; Boey, F. Y. C.; Zhang, H. *Adv. Mater.* **2008**, *20*, 4873.

(13) Wang, H. T.; Nafday, O. A.; Haaheim, J. R.; Tevaarwerk, E.; Amro, N. A.; Sanedrin, R. G.; Chang, C. Y.; Ren, F.; Pearton, S. J. *Appl. Phys. Lett.* **2008**, *93*.

(14) Basnar, B.; Willner, I. *Small* **2009**, *5*, 28.

(15) Hoogenboom, J. P.; Vossen, D. L. J.; Faivre-Moskalenko, C.; Dogterom, M.; van Blaaderen, A. *Appl. Phys. Lett.* **2002**, *80*, 4828.

(16) Grigorenko, A. N.; Roberts, N. W.; Dickinson, M. R.; Zhang, Y. *Nat. Photonics* **2008**, *2*, 365.

(17) Xia, Y.; Whitesides, G. *Ann. Rev. Mater. Sci.* **1998**, *28*, 153.

(18) He, H. X.; Huang, W.; Zhang, H.; Li, Q. G.; Li, S. F. Y.; Liu, Z. F. *Langmuir* **2000**, *16*, 517.

(19) Ahn, J. H.; Kim, H. S.; Lee, K. J.; Jeon, S.; Kang, S. J.; Sun, Y. G.; Nuzzo, R. G.; Rogers, J. A. *Science* **2006**, *314*, 1754.

(20) Minelli, C.; Geissbuehler, I.; Eckert, R.; Vogel, H.; Heinzelmann, H.; Liley, M. *Colloid Polym. Sci.* **2004**, *282*, 1274.

(21) Fan, Z. Y.; Ho, J. C.; Jacobson, Z. A.; Yerushalmi, R.; Alley, R. L.; Razavi, H.; Javey, A. *Nano Lett.* **2008**, *8*, 20.

(22) Gao, M. Y.; Sun, J. Q.; Dulkeith, E.; Gaponik, N.; Lemmer, U.; Feldmann, J. *Langmuir* **2002**, *18*, 4098.

(23) Park, J.; Fouche, L. D.; Hammond, P. T. *Adv. Mater.* **2005**, *17*, 2575.

(24) Gotschy, W.; Vonmetz, K.; Leitner, A.; Aussenegg, F. R. *Appl. Phys. B* **1996**, *63*, 381.

(25) Werts, M. H. V.; Lambert, M.; Bourgoin, J. P.; Brust, M. *Nano Lett.* **2002**, *2*, 43.

(26) Hua, F.; Cui, T. H.; Lvov, Y. *Langmuir* **2002**, *18*, 6712.

(27) Xia, D. Y.; Brueck, S. R. J. *Nano Lett.* **2004**, *4*, 1295.

(28) Hung, A. M.; Micheel, C. M.; Bozano, L. D.; Osterbur, L. W.; Wallraff, G. M.; Cha, J. N. *Nat. Nanotechnol.* **2010**, *5*, 121.

(29) Hua, F.; Shi, J.; Lvov, Y.; Cui, T. *Nano Lett.* **2002**, *2*, 1219.

(30) Jamshidi, A.; Neale, S. L.; Yu, K.; Pauzauskie, P. J.; Schuck, P. J.; Valley, J. K.; Hsu, H. Y.; Ohta, A. T.; Wu, M. C. *Nano Lett.* **2009**, *9*, 2921.

(31) Vossmeyer, T.; Jia, S.; DeIonno, E.; Diehl, M. R.; Kim, S. H.; Peng, X.; Alivisatos, A. P.; Heath, J. R. *J. Appl. Phys.* **1998**, *84*, 3664.

(32) Wilbur, J. L.; Kumar, A.; Kim, E.; Whitesides, G. M. *Adv. Mater.* **1994**, *6*, 600.

(33) Xia, Y. N.; Mrksich, M.; Kim, E.; Whitesides, G. M. *J. Am. Chem. Soc.* **1995**, *117*, 9576.

(34) Xia, Y. N.; Whitesides, G. M. *Langmuir* **1997**, *13*, 2059.

(35) Harirchian-Saei, S.; Wang, M. C. P.; Gates, B. D.; Moffitt, M. G. *Langmuir* **2010**, *26*, 5998.

(36) Harirchian-Saei, S.; Wang, M. C. P.; Gates, B. D.; Moffitt, M. G. *Langmuir* **2012**, *28*, 10838.

(37) Krausch, G.; Dai, C.; Kramer, E.; Bates, F. *Phys. Rev. Lett.* **1993**, *71*, 3669.

(38) Walheim, S.; Boltau, M.; Mlynek, J.; Krausch, G.; Steiner, U. *Macromolecules* **1997**, *30*, 4995.

(39) Kielhorn, L.; Muthukumar, M. *J. Chem. Phys.* **1999**, *111*, 2259.

(40) Walheim, S.; Ramstein, M.; Steiner, U. *Langmuir* **1999**, *15*, 4828.

(41) Rockford, L.; Liu, Y.; Mansky, P.; Russell, T.; Yoon, M.; Mochrie, S. *Phys. Rev. Lett.* **1999**, *82*, 2602.

(42) Fukunaga, K.; Elbs, H.; Krausch, G. *Langmuir* **2000**, *16*, 3474.

(43) Sehgal, A.; Ferreiro, V.; Douglas, J.; Amis, E.; Karim, A. *Langmuir* **2002**, *18*, 7041.

(44) Zong, Q.; Li, Z.; Xie, X. *Macromol. Chem. Phys.* **2004**, *205*, 1116.

(45) Heriot, S. Y.; Jones, R. A. L. *Nat. Mater.* **2005**, *4*, 782.

(46) Raczkowska, J.; Cyganik, P.; Budkowski, A.; Bernasik, A.; Rysz, J.; Raptis, I.; Czuba, P.; Kowalski, K. *Macromolecules* **2005**, *38*, 8486.

(47) Andrew, P.; Huck, W. *Soft Matter* **2007**, *3*, 230.

(48) Park, L.; Munro, A.; Ginger, D. *J. Am. Chem. Soc.* **2008**, *130*, 15916.

(49) Jaczewska, J.; Budkowski, A.; Bernasik, A.; Raptis, I.; Moons, E.; Goustouridis, D.; Haberko, J.; Rysz, J. *Soft Matter* **2009**, *5*, 234.

(50) Wang, C.-W.; Moffitt, M. G. *Langmuir* **2004**, *20*, 11784.

(51) Cheyne, R. B.; Moffitt, M. G. *Langmuir* **2005**, *21*, 10297.

(52) Yusuf, H.; Kim, W.-G.; Lee, D.-H.; Guo, Y.; Moffitt, M. G. *Langmuir* **2007**, *23*, 868.

(53) Yusuf, H.; Kim, W.-G.; Lee, D.-H.; Aloshyna, M.; Brolo, A. G.; Moffitt, M. G. *Langmuir* **2007**, *23*, 5251.

(54) Henglein, A. *Chem. Rev.* **1989**, *89*, 1861.

(55) Moffitt, M.; McMahon, L.; Pessel, V.; Eisenberg, A. *Chem. Mater.* **1995**, *7*, 1185.

(56) Mayer, A. B. R. *Polym. Advan. Technol.* **2001**, *12*, 96.

(57) Li, X. L.; Zhang, J. H.; Xu, W. Q.; Jia, H. Y.; Wang, X.; Yang, B.; Zhao, B.; Li, B. F.; Ozaki, Y. *Langmuir* **2003**, *19*, 4285.

(58) Jia, H. Y.; Zeng, J. B.; Song, W.; An, J.; Zhao, B. *Thin Solid Films* **2006**, *496*, 281.

(59) Zhang, F. X.; Guan, N. J.; Li, Y. Z.; Zhang, X.; Chen, J. X.; Zeng, H. S. *Langmuir* **2003**, *19*, 8230.

(60) Hu, X. X.; Hu, C.; Qu, J. H. *Mater. Res. Bull.* **2008**, *43*, 2986.

(61) Pierson, J. F.; Rousselot, C. *Surf. Coat. Tech.* **2005**, *200*, 276.

(62) Guo, Y.; Moffitt, M. *Chem. Mater.* **2007**, *19*, 6581.

(63) Gast, A. P. *Langmuir* **1996**, *12*, 4060.

(64) McConnell, G. A.; Gast, A. P.; Huang, J. S.; Smith, S. D. *Phys. Rev. Lett.* **1993**, *71*, 2102.

(65) Mcconnell, G. A.; Lin, E. K.; Gast, A. P.; Huang, J. S.; Lin, M. Y.; Smith, S. D. *Faraday Discuss.* **1994**, *98*, 121.

(66) Chen, H. L.; Lin, S. Y.; Huang, Y. Y.; Chiu, F. C.; Liou, W.; Lin, J. S. *Macromolecules* **2002**, *35*, 9434.

(67) Higuchi, T.; Tajima, A.; Yabu, H.; Shimomura, M. *Soft Matter* **2008**, *4*, 1302.

(68) Kumar, S.; Jouault, N.; Benicewicz, B.; Neely, T. *Macromolecules* **2013**, *46*, 3199.

Highlights

- Simultaneous patterning of different inorganic nanoparticle types is demonstrated by spin-casting blend solutions containing nanoparticles functionalized with immiscible polymer brush layers onto microcontact printed surfaces.
- By varying spin speed, polymer concentration, and blend composition, we obtain alternating stripes of cadmium sulfide quantum dots and silver nanoparticles dispersed in different polymer phases in a single spin-casting step.
- Key to this method is the addition of homopolymers to blend solutions, which increases free volume between the nanoparticles and prevents their gelation during spin-casting.

Graphical Abstract